

Pore Characteristics and Fractal Dimension Analysis of Tectonic Coal and Primary-Structure Coal: A Case Study of Sanjia Coal Mine in Northern Guizhou

Huaying Lin, Shixiang Tian,* Anjun Jiao, Zuoyong Cao, Kai Song, and Yihuai Zou



Cite This: *ACS Omega* 2022, 7, 27300–27311



Read Online

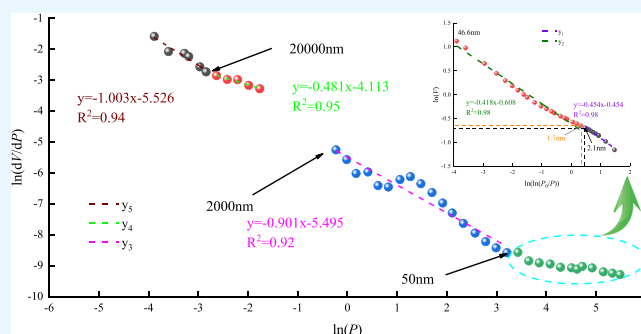
ACCESS |

Metrics & More

Article Recommendations

ABSTRACT: Understanding the pore heterogeneity of tectonic coal and primary-structure coal is of great significance for predicting and preventing tectonic coal. This study adopts the low-temperature nitrogen adsorption method, mercury injection experiment, and other methods, combined with fractal theory, to quantitatively analyze the pore distribution of coal samples inside and outside the outburst cavities of the Sanjia coal mine. The experiments have shown that the contents of aliphatic functional groups and hydrogen in tectonic coal are higher than those of aromatic structural functional groups. Raw coal has more straight chains than side chains, whereas aliphatic hydrocarbon mostly has short chains, and the branching degree is high. Soft and primary-

structure coals have similar elemental content and tectonic effects endow the coal with better connectivity. The pores are filled with particles and flakes, and the surfaces of tectonic coal have more pores and fissures on them. According to the experimental curve, the pores are divided into five types. The pore size of primary-structure coal is mainly type II pores, and the pore size distribution of tectonic coal is relatively wide, with the majority being class I and class II pores. The specific surface area of tectonic coal is 60.7% more than that of primary-structure coal. The box fractal dimension of coal decreases with the increase in scanning electron microscopy (SEM) magnification. The minimum fractal dimension of tectonic coal is 2.49, which is 7.8% lower than the peak of 2.70. It can be seen from the fractal dimension that the fractal dimensions of pore types II, III, and IV are rougher.



1. INTRODUCTION

Coal is a kind of porous medium containing a large number of surface areas. Gas mainly exists in coal seams in a free and adsorbed state and in a mutual equilibrium state in a stable environment.^{1–5} The difference in the pore structure of coal makes the porosity, permeability, and adsorption capacity of coal significantly different and even affects the diffusion and seepage of coal gas. Therefore, studying the pore structure of coal is of great significance to understand the mechanism of coal gas migration and mine disasters.

At present, the research methods of coal pores mainly include scanning electron microscopy,⁶ high-pressure mercury injection,⁷ and low-temperature nitrogen adsorption.^{8,9} Mercury injection is based on the characteristics of the mercury injection curve and mercury injection pressure, which can effectively reflect the characteristics of coal pores.^{10,11} Scanning electron microscopy (SEM) is a method of transmission and optical microscopic observation.^{12–15} By scanning the synaptic points on the surface of the measured object by electron beam, the microscopic morphology image of the material is generated according to the surface fluctuation. In contrast, Pan et al.'s method is based on the capillary condensation phenom-

on,^{16–18} i.e., nitrogen begins to condense in micropores, and the pore volume and diameter distributions are analyzed.

Many scholars have carried out different types of research using the methods described above. For instance, Liu¹⁹ used cryogenic liquid adsorption and mercury intrusion experiments to study the fractal dimension of the pore structure of coal samples. Furthermore, Chen²⁰ used the Menger sponge model to analyze the fractal characteristics of coal pore structures with different degrees of metamorphism, indicating that the fractal characteristics of coal pores have a certain influence on the gas adsorption characteristics. Mangi²¹ systematically analyzed the influence of pore size distribution and fractal dimension on the adsorption and desorption values using SEM and low-pressure adsorption of N₂ and CO₂, which was done on surfaces mainly consisting of micro- and mesopores. Tu²² found that structural

Received: April 12, 2022

Accepted: July 4, 2022

Published: July 25, 2022



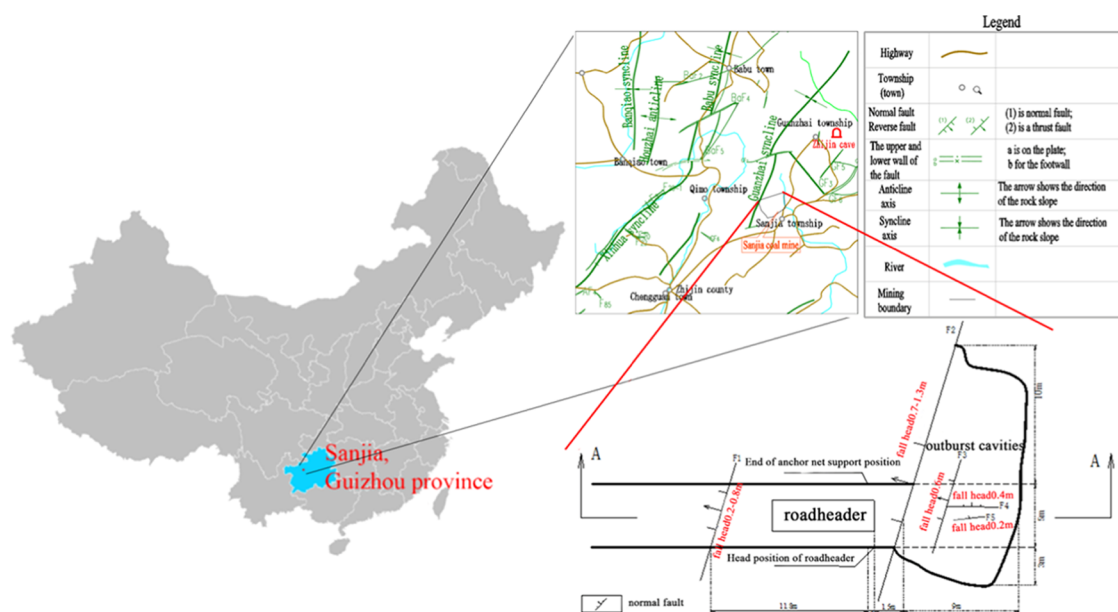


Figure 1. Map of coal specimen sampling sites.

destruction/pulverization first modifies the small pores and above pores in coal. Research by Ye²³ has shown that under the effect of brittle structure reformation, the formed fragmented coal has a pore fracture structure advantage ratio that determines the permeability of the reservoir.

Domestic and foreign scholars have studied the pore structure of coal affected by tectonic action. To study the influence of tectonic action on pore characteristics in detail, different experiments are needed to analyze different pore sizes. According to previous studies,^{24–29} in a certain range, the coal morphology characteristics and the pore structure have self-similarity, and fractal geometry can be used to describe the disorder and irregularity of matter. Recently, research has revealed that there is a strong relation between fractal dimension and pore structure.³⁰

This paper explores the law of structural effects on pore changes in coal. First, the influence of coal chemical composition and functional groups on gas adsorption was studied by industrial analysis and Fourier transform infrared spectroscopy. Second, through the scanning electron microscope, intuitive analysis of coal pore fracture, combined with mercury intrusion test and liquid nitrogen adsorption analysis of coal pore volume and specific surface area distribution, was performed. Finally, the fractal theory quantitatively analyzes the complexity and heterogeneity of pores, so as to better explain the influence of coal on gas adsorption after tectonism.

2. COAL SAMPLES AND EXPERIMENTS

After the formation of a coal seam, the tensile and fracture activities in the tectonic movement cause a large amount of coal seam gas to dissipate. Different levels of tectonic activity and tectonic stress field control the scope and intensity of tectonic action and the occurrence and distribution of coal seam gas in different ranges. At the same time, it also controls the migration conditions of coal seam and the destruction conditions and scope of coal structure. Due to the different tectonic stress fields and the internal stress state in the formation process of different types of geological structures, the occurrence, structure, physical properties, and fracture development of coal seams and caprocks

are different, which affects the preservation of gas. The zone where tectonic stress is relatively concentrated is the main place where gas outburst occurs, i.e., where rock is deformed and tectonic stress is not fully released. The regional distribution of coal and gas outburst in coalfields and mines is predetermined by the uneven distribution of the tectonic stress field. The outburst occurs at the place where the tectonic stress increases, with the compressive and torsional structures particularly more prone to gas outbursts. On the one hand, these structures are conducive to the formation and development of tectonic coal. On the other hand, due to the concentration of tectonic stress, which makes the coal seam in a state of strong pressure and reduces the permeability of the coal seam, thus helping to form high-pressure gas with a large pressure gradient in the coal seam.

2.1. Sample Collection and Coal Analyses. The Sanjia coal mine belongs to the Sanjia exploration area, located in Sanjia Township, northeast of Zhijin County, Guizhou Province, the southwest section of the Guiyang complex structural deformation zone, and the southeastern wing of the southwest section of the Guanzhai syncline, as shown in Figure 1. It is a monoclinic structure as a whole, with the strata trending northeast and leaning northwest, with a dip angle of approximately 10°. The faults found in the mining area are located in the southern part of the mining area and its edges, and the formation behavior has changed owing to the influence of the faults. The sampling location was selected at the driving face of the 41 601 transportation lane, which was located near the northern boundary of the mining area, the lowest section of the M16 coal seam in the fourth district sublevel, as shown in Figure 1. Tectonic coal (TC) samples were taken from the protruding holes, and primary-structure coal (PSC) samples were taken from the outside of the protruding holes. The two kinds of coal samples were 5 kg each.

The coal samples were collected at the sampling site, packaged, and sent to the laboratory immediately to prevent oxidation. In the laboratory, coal samples were first crushed and then screened to the appropriate particle size. According to GB/T 214-2007 and SN/T 4764-2017, the components of coal samples were determined by an industrial analyzer and an

Table 1. Composition Table of the Coal Samples^a

ingredient sample	industrial analysis				elementary analysis				
	FCad (%)	Aad (%)	Vad (%)	Mad (%)	C	H	N	S	O
TC	82.9	6.1	5.4	4.6	90.15	3.87	1.51	0.42	4.05
PSC	81.7	9.3	4.7	4.3	90.36	3.69	1.65	0.38	3.92

^aMad = moisture content (wt %, air dry basis), Aad = ash yield (wt %, air dry basis), Vad = volatile matter (wt %, air dry basis), FCad = fixed carbon (wt %, air dry basis).

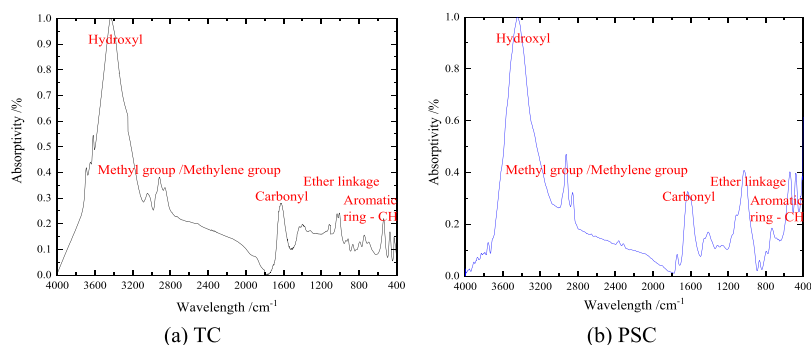


Figure 2. Infrared spectrum curve of the coal sample.

elemental analyzer, respectively. In the industrial analysis experiment, a 5E-MAG6700 Kaiyuan industrial analyzer was used to test the contents of moisture, ash, and volatile matter in coal, and the fixed carbon content was obtained by subtraction. The instrument mainly relied on the calorimeter and the microbalance to heat the sample and continuously detect the quality change of the sample to obtain the main experimental parameters. The moisture contents of tectonic coal and primary-structure coal are 4.6 and 4.3%, the ash yields of tectonic coal and primary-structure coal are 6.1 and 9.3%, the volatile matter variations are 5.4 and 4.7%, and fixed carbon variations are 82.9 and 81.3%, respectively. The composition of the coal samples can be seen in Table 1.

2.2. Experimental Procedure. Infrared spectroscopy is a material analysis method based on the difference in the infrared light absorption of different molecules. The infrared absorption spectrum is the image formed by the continuous relative motion of molecules at the equilibrium position. The components of each substance are different. When the detected substance moves at the same position at the same frequency, and the molecular vibration energy corresponds to the photon energy in the infrared light, the molecules undergo a transition, and the peripheral electrons of the molecule absorb the energy in the incident light from the low level to the high level. There is a “band” in the vibration spectrum, and the measured material composition can be obtained by analyzing the spectrum.

First, for the scanning electron microscopy experiment, the collected coal samples were cut into pieces with the height and diameter not exceeding 145 and 250 mm, respectively. Then, the cut surface of the sample was ground and cut. A conductive glue was then applied to the cut surface of the sample before pasting this surface on the sample holder. A blower was then used to blow away the attachments or debris on the sample surface. Finally, the purged samples were treated under vacuum drying and conduction.

To reduce the influence of moisture on the test, the coal sample was dried at 100 °C before performing the mercury intrusion experiment using an Auto Pore 9505 mercury intrusion meter. When the mercury intrusion method was

used for testing, mercury entered the cracks first in the low-pressure stage. As the pressure increased, mercury began to enter the pores when the pressure was greater than the capillary force of the pore throat. For cylindrical holes, the following equation was satisfied

$$P = -4\alpha \cos \theta / d \quad (1)$$

where P is the pressure of the pressed mercury (MPa), α is the surface tension of mercury (485 mN/m), θ is the contact angle between the mercury and the surface of the coal sample, taken as 130°, and d is the pore diameter (nm).

The experimental test instrument used was a 3H-2000PS2 analyzer of the specific surface area and pore size. The measurement temperature was 77.3 K. The test pore size range was 0.35–500 nm. The samples were manually screened to eliminate the mineral impurities contained in the samples and the fracture and structural fracture caused by human activities and to minimize the possibility of these characteristics affecting the measurement results. Then, the sample was crushed and sieved to 60–80 mesh pulverized coal sample. Single-layer adsorption was obtained according to the multimolecular layer adsorption formula to analyze the specific surface area, pore size, and pore volume distribution.

The van der Waals force and the gas–liquid two-phase surface tension mainly affect gas adsorption by coal. The main force in the adsorption process is affected by pressure. The van der Waals forces play a major role in the low-pressure stage. As the pressure increases, the effect of the gas–liquid two-phase surface tension becomes increasingly noticeable. The critical point of the two forces occurs when $A = -1/3$. When $A > -1/3$, the van der Waals force is much larger than the surface tension. When $A < -1/3$, the surface tension has a significant effect.

3. ANALYSIS OF COAL FUNCTIONAL GROUPS

The infrared spectrum of coal is a mixed peak of various organic and inorganic minerals, and the peak shapes cover each other and overlap. By analyzing the original data of the two coal samples, the infrared spectra of the two coal samples are obtained, and the spectra are shown in Figure 2.

Table 2. Semiquantitative Parameters Based on Infrared Spectroscopy

semiquantitative parameters	parameter calculation suction	peak harvesting calculation (cm ⁻¹)
aromaticity <i>I</i>	bending vibration of aromatic C–H/aliphatic C–H	(700~900)/(2800–3000)
condensation DOC	bending vibration of aromatic C–H/aromatic C=C	(700–900)/(1490–1600)
fat chain length	CH ₂ /CH ₃	2920/2950
hydrocarbon generation potential HGP	fat C–H/(fat + aromatic C=C)	(2800–3000)/[(2800–3000) + (1490–1600)]
maturity <i>C</i> _{sd}	aromatic C=C/(aromatic C=C + COOH)	(1490–1600)/[(1490–1600) + 1700]

Fourier transform infrared (FTIR) spectroscopy has been widely used in the study of coal chemical structure and coal evolution. However, due to the complex molecular structure of coal and the influence of sample preparation and experimental equipment, the technology can only be used for qualitative analysis in the early stage and cannot complete quantitative research. With the assistance of data processing software, the following structural parameters can be semiquantitatively analyzed using the ratio of functional group subpeak area so as to analyze the structural changes of coal in the metamorphic evolution process.³¹ The calculation of structural parameters is shown in Table 2.

Maturity *C*_{sd} is used to evaluate the maturity of organic matter during coal metamorphism. The length of the fat chain represents the length and branching degree of the fat chain in coal. Hydrocarbon generation potential is usually used to evaluate kerogen hydrocarbon generation potential. Aromaticity is used to characterize the degree of aromatization of the coal structures. The higher the aromaticity, the higher the degree of aromatization. The degree of condensation represents the degree of condensation of aromatic rings in the coal structures. The parameter calculation results are shown in Table 3.

Table 3. Calculated Value of Coal Sample Structure Parameters

sample	parameter				
	<i>I</i>	DOC	<i>A</i> _{CH₂} / <i>A</i> _{CH₃}	HGP	<i>C</i> _{sd}
TC	0.318	1.560	0.850	0.807	0.969
PSC	0.298	1.010	0.916	0.738	0.976

The value of *I* of tectonic coal is larger than that of primary-structure coal, indicating that the aliphatic functional group of tectonic coal is higher than that of the aromatic structural functional group. The DOC of tectonic coal is higher than that of primary coal, and the hydrogen content is higher than that of primary coal, indicating that the outburst coal has better hydrocarbon generation potential, which is consistent with the calculated HGP value. The *A*_{CH₂}/*A*_{CH₃} raw coal is relatively low, and the maturity is slightly higher than that of tectonic coal, indicating that the raw coal has more straight chains than side chains, and the aliphatic hydrocarbons are mostly short chains and have a high branched degree. However, on the whole, the structural parameters have little difference.

4. COAL SAMPLE PORE SIZE AND SPECIFIC SURFACE AREA

4.1. SEM Analysis of the Coal Sample. **4.1.1. Pore Profile Analysis.** The primary structure of the coal had good homogeneity and integrity, and three types of micropores could be seen in the coal, namely, pores, cell pores, and mold pores.³² Stomatal pores were metamorphic pores formed by the effects of “gas generation” and “accumulation gas” during coal

metamorphism at the coal formation stage. These pores had different shapes, such as subcircular, ellipsoidal, and irregular shapes. The distribution of pores was concentrated, and some of them were produced in groups. The size of the pores varied but was essentially below 10 μm. The pores were fundamentally not connected. The pores were often filled with granular and flake-like detrital minerals, minerals, and organic matter, which were formed owing to the difference in the hardness due to the compressive stress during coal formation. In the process of coal formation, some imprint pits were formed under the action of compressive stress. These imprint pits were mold holes, which were a type of mineral pores. The pore shape of the mold was highly complex. The pores were not connected and were all “dead holes.” The pore diameters were generally less than 20 μm.

Compared with Figure 3a,d, owing to the tectonic stress field and its evolution, the coal body was destroyed, and a large number of broken particles were formed. The grains were combined and stacked to form strips, sheets, or semicircular pores between the grains. The holes varied in size, but most of them were 1–10 μm. The pore diameters were also significantly different, with values ranging from 0.5 to 5.0 μm. Due to the tectonic stress, tectonic coal had more microcracks than primary-structure coal. The pores were well-developed and concentrated, and there was much connectivity between pores.

4.1.2. Box-Counting Dimension. The box-counting dimension in fractal dimension can reflect the distribution pattern of microfractures in three-dimensional space from the spatial possession ability, and quantitatively analyze the heterogeneity and complexity of microfractures in space. Then, the difference in the coal reservoir permeability is revealed. The fractal curve is placed in a box with *r* edges. Some fractal curves do not occupy the space of small boxes, and small boxes cover some curves. The number of empty and nonempty boxes are noted, and *N*(*r*) is used to represent the number of nonempty boxes. Reducing the size of the box increases *N*(*r*). When *r* approaches 0, the fractal dimension can be obtained

$$D = \lim_{r \rightarrow 0} \frac{\ln N(r)}{\ln(1/r)} \quad (2)$$

where *D* is the surface fractal dimension.

According to image recognition and box fractal dimension, the python platform is used to build a platform for calculating the fractal dimension in Figure 3a,l.

The fractal dimension of each coal sample with different magnification boxes is summarized, and the summary diagram is shown in Figure 4.

The fractal dimension of the coal box showed a decreasing trend with the increase in magnifications of SEM. The minimum fractal dimension of primary-structure coal was 2.49, which was 7.8% lower than the peak value of 2.70. The fractal dimension of tectonic coal remained above 2.6. Due to the small magnifications, the microcracks were more obvious than the pores. When the magnifications were large enough, the pore

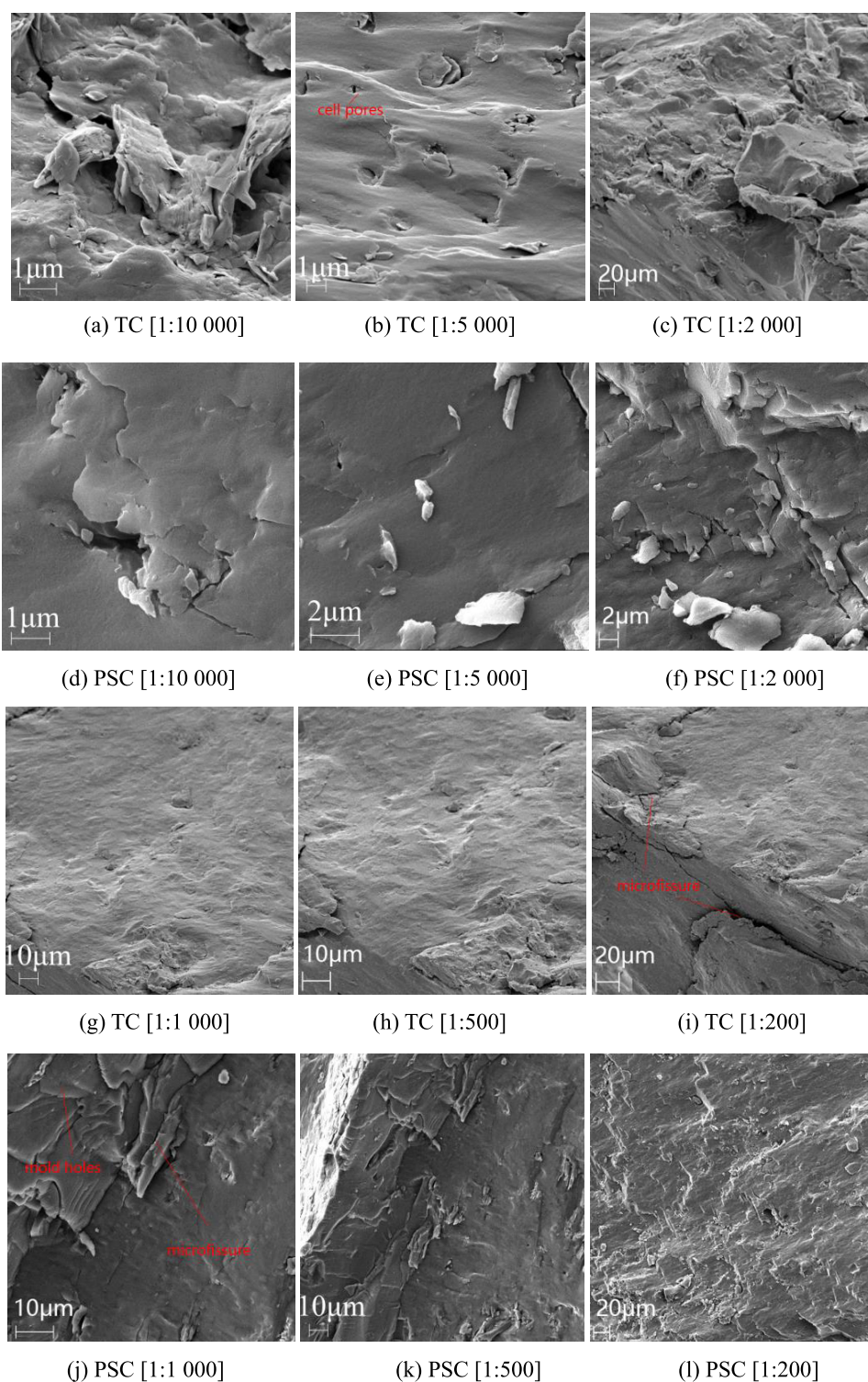


Figure 3. Pore types of different rank coal samples from SEM images.

performance was more prominent, and the range of microcracks in the figure decreased, which reduced the box dimension. The complexity of fractures and pores can be analyzed simply according to changes. Since a small amount of pulverized coal remained on the surface of primary structure coal before the experiment, and the section is stepped, the surface reflection is serious relative to tectonic coal, resulting in the 200 and 500 magnifications box dimension is higher than tectonic coal, as shown in Figure 5

4.2. N₂ Isothermal Adsorption–Desorption Curves.

4.2.1. Pore Type Analysis. In liquid nitrogen adsorption experiments, if the adsorption–desorption is not completely reversible, the adsorption–desorption isotherms do not coincide. This phenomenon is called the hysteresis effect, that is, the results are related to the process, and often occurs in type IV adsorption equilibrium isotherms. The low specific pressure region is related to the monolayer adsorption. Due to the reversibility of monolayer adsorption, there is no hysteresis

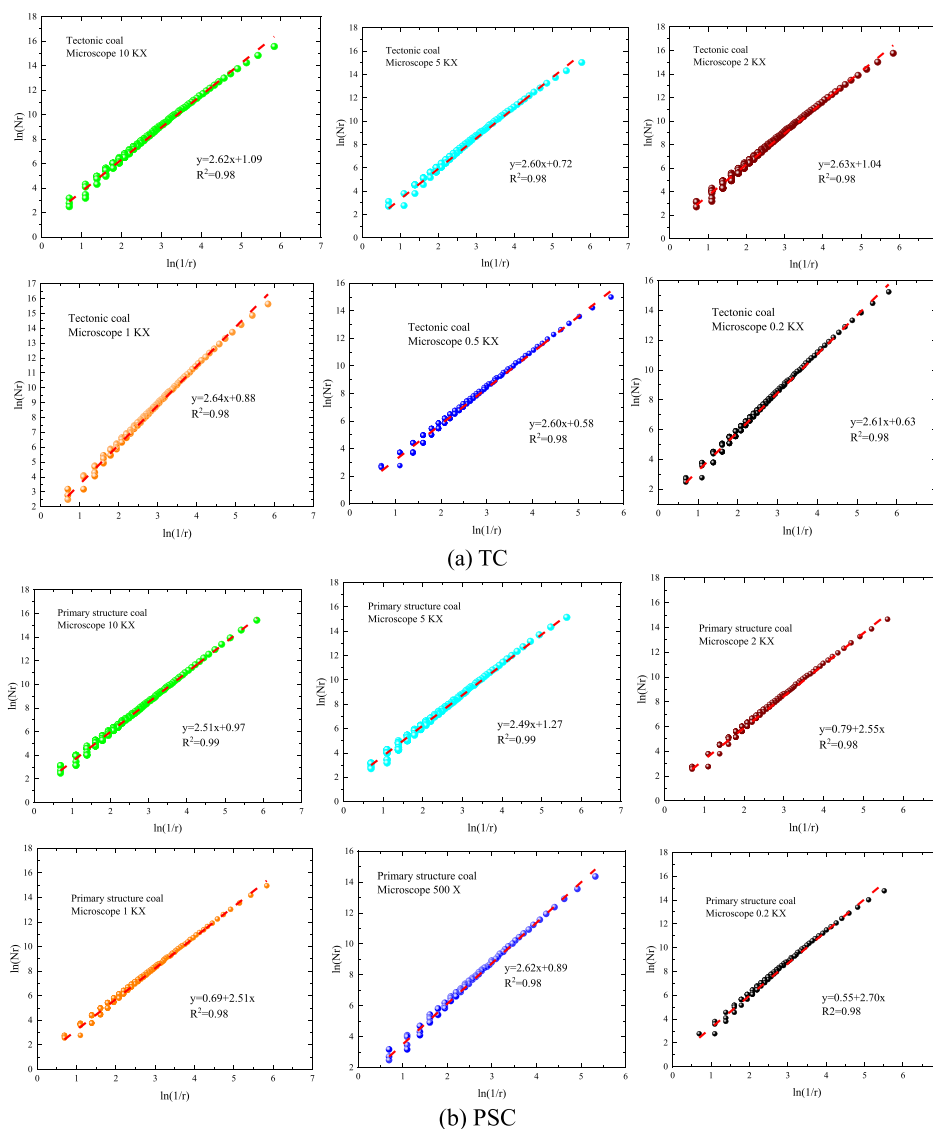


Figure 4. $\ln(1/r) - \ln(N_r)$ curves at different magnifications.

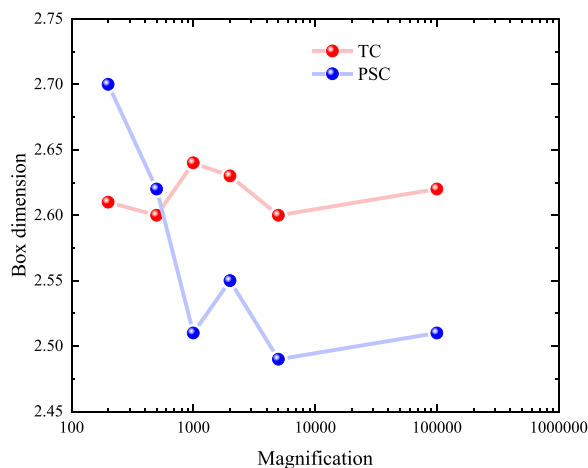


Figure 5. Box dimension of scanning electron microscopes.

phenomenon in the low specific pressure region. According to the adsorption–desorption curve, four types of pore structures are divided, and the specific pore types are shown in Table 4.

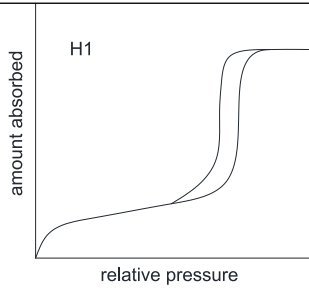
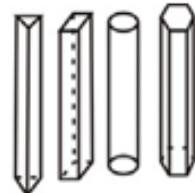
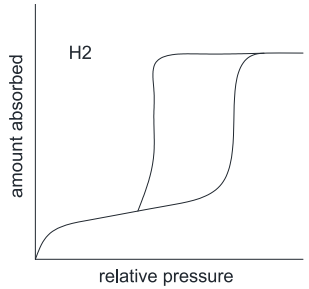
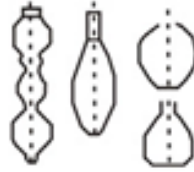
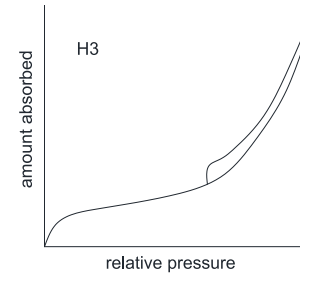
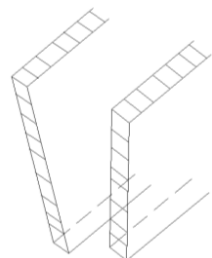
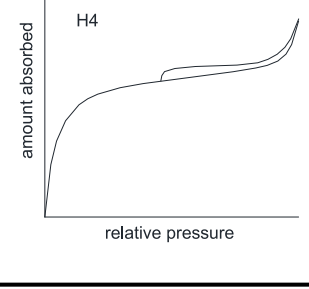

As shown in Figure 6, the adsorption curve of the coal sample increases steadily when P/P_0 is small and increases rapidly when P/P_0 is close to 1.0. When the relative pressure is 0.45–1.0, there is an obvious hysteresis loop. When P/P_0 is around 0.5, the inflection point appears, indicating that the pore morphology was ink bottle-shaped or unilaterally closed fine bottleneck pores. The pores with a diameter greater than 10 nm have good connectivity, and the pore morphology may be cylindrical and parallel plate-like with both sides open.

4.2.2. Volume Fractal Dimensions. According to the experimental data on nitrogen adsorption, FHH fractal dimension model was used to calculate the fractal dimension of the coal pore volume. The fractal dimension samples are determined by the FHH fractal model.

$$\ln\left(\frac{V}{V_0}\right) = A \ln\left[\ln\left(\frac{P_0}{P}\right)\right] + C \quad (3)$$

where V is the coal sample adsorption volume (mL) under pressure P , V_0 is the adsorption volume of the unit molecular layer (mL), P_0 is the saturated vapor pressure (Pa), P is the balance pressure (Pa), A is a linear constant, and C is a constant.

Table 4. Summary of Pores Types

Pores type	Adsorption-desorption curve	Pores schematic
cylinder pores	 <p>H1</p> <p>amount absorbed</p> <p>relative pressure</p>	
cylinder & spherical pores	 <p>H2</p> <p>amount absorbed</p> <p>relative pressure</p>	
disordered lamellar pore structures, silt & wedge, shape pores	 <p>H3</p> <p>amount absorbed</p> <p>relative pressure</p>	
parallel plate-like pores	 <p>H4</p> <p>amount absorbed</p> <p>relative pressure</p>	

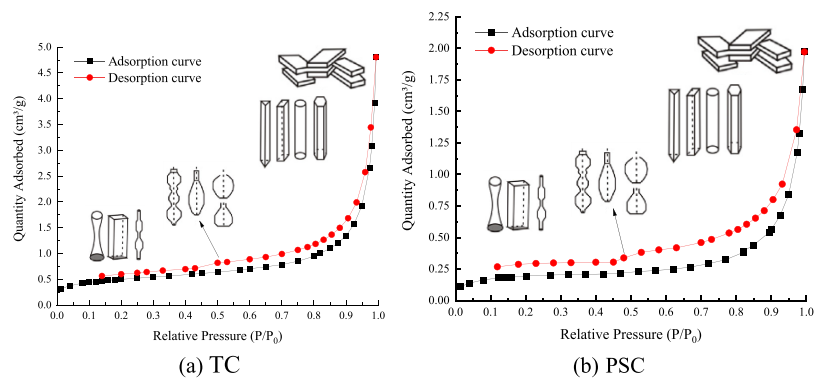


Figure 6. Adsorption-desorption curves of different coal samples.

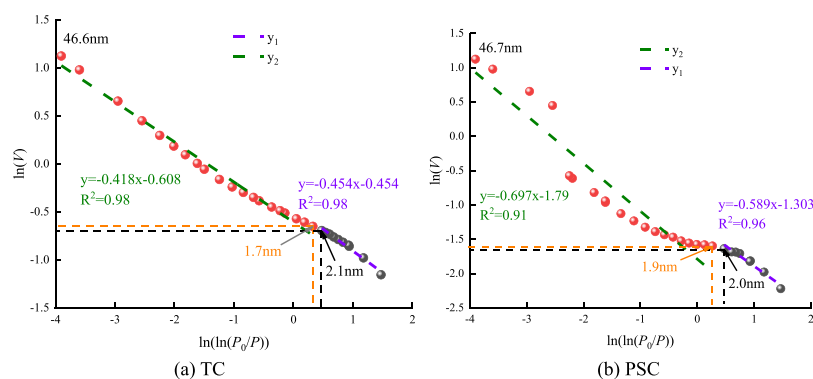


Figure 7. Representative plots of $\ln V$ vs $\ln(\ln(P_0/P))$ reconstructed from the N_2 adsorption analysis of different coal samples.

According to the experimental data of nitrogen adsorption, using the FHH fractal dimension model, there are two conventional methods to determine the fractal dimension of the surface and pore volume of the coal sample j : $D = A + 3$ and $D = 3A + 3$. However, the calculation results of $D = 3A + 3$ are often less than 2, which does not meet the range of fractal dimensions. Therefore, $D = A + 3$ is used to determine the volume fractal dimensions of micropores and mesopores.

Through the FHH model, the linear fitting of $\ln V$ and $\ln(\ln(P_0/P))$ is carried out. The curve is shown in Figure 7. When the pore diameter is 2 nm, the curve is divided into two sections. The fractal dimension of each segment is calculated according to Figure 7. The results are shown in Table 5. It can be

Table 5. Pore Volume Fractal Dimensions from the N_2 Adsorption Data of Coal Samples^a

sample	γ_1			γ_2		
	A	D_1	R^2	A	D_2	R^2
TC	-0.454	2.546	0.98	-0.418	2.582	0.98
PSC	-0.589	2.411	0.96	-0.697	2.303	0.91

^a D_1 is class I pore volume fractal dimension. D_2 is the fractal dimension of the type II pore volume.

seen from Table 5 that $D_1 D_2$ and the value of primary-structural coal are relatively low. There is no obvious correlation between D_1 and D_2 , indicating that different pore types have different effects on pore volume fractal characteristics.

4.3. Pore Size Distribution of MIP. **4.3.1. Mercury Curve Analysis.** It can be seen from Figure 8 that the maximum injection amounts of mercury in tectonic coal and primary-structure coal are 0.064 and 0.02556 mL/g, respectively. In the early stages of mercury removal, a small part of the mercury

advancing and retreating curves overlapped with the coal sample. Among them, the lagged loop was larger, the pores were more open, and the connectivity was higher. The mercury intake of primary-structure coal was much smaller than that of structural coal, the lagged loop formed by the mercury advancing and retreating curves was smaller, the pores were less open, and the connectivity was poorer.

4.3.2. Geometric Fractal Dimension. Due to the unique complexity and heterogeneity of coal pore structure, it is difficult to accurately and quantitatively describe and characterize it using traditional methods. However, fractal theory can effectively be used to study and describe the pore morphology of coal. Mandelbrot³³ first proposed the fractal theory, and it is widely used in the analysis of surface characteristics of self-similar substances. The size of the fractal dimension reflects the complexity and heterogeneity of the coal pores. The larger the fractal dimension, the less regular the pore shapes are and the rougher the surface is.

After mercury enters the pores, the total pore volume under the current pressure equals the amount of mercury entering the pores. Therefore, the relationship between the pore volume gradient and the pressure and fractal dimension can be obtained through the relationship between the pore volume and fractal dimension³⁴

$$\frac{dV}{dP} \propto P^{D-1} \quad (4)$$

Take the logarithm on both sides of the equal sign to obtain

$$D = 4 + \frac{\ln\left(\frac{dV}{dP}\right)}{\ln(P)} \quad (5)$$

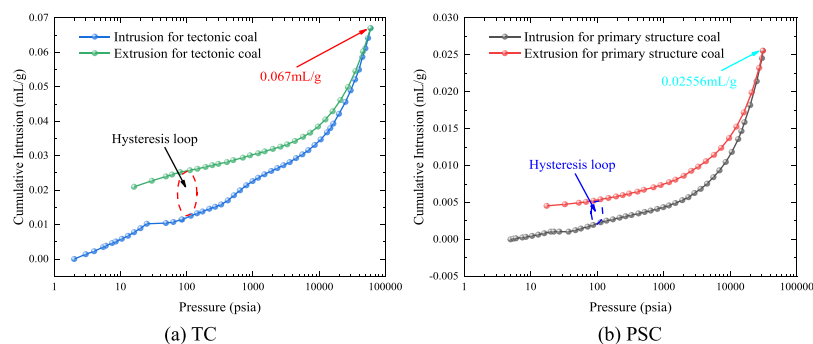


Figure 8. Mercury inflow and mercury withdrawal curves.

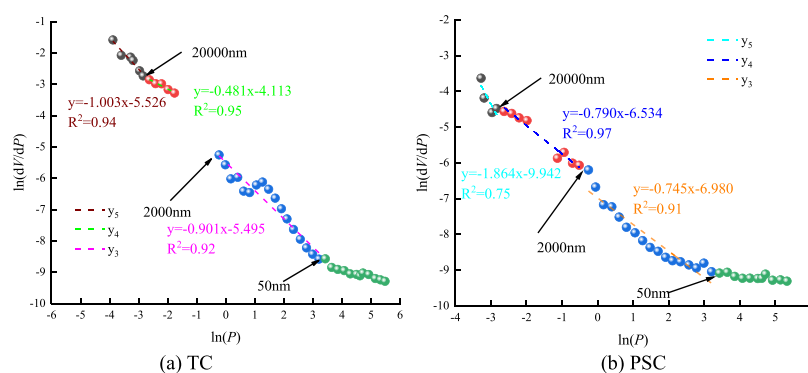


Figure 9. dV/dP and P logarithmic graph of the coal sample.

By processing the experimental data, a scatter plot can be drawn with $\lg(dV/dP)$ as the ordinate and $\lg(P)$ as the abscissa, and each point can fit the curve. The double logarithm diagram of $\lg(dV/dP)$ and $\lg(P)$ (as shown in Figure 9) shows that the curve is divided into four sections when the pore size is 2000, 2000, and 50 nm. To better analyze the pore characteristics of coal samples, the pore size is divided into four sections according to the inflection point of the mercury intrusion test: V (~ 20000 nm), IV (20000–2000 nm), III (2000–50 nm). Because the error of pores is less than 50 nm, the classification is not continued here. Except for the curve less than 50 nm, each segment is fitted.

Owing to the strong heterogeneity of coal, the fractal dimension of pores in different pore sizes is different. It is difficult to represent the overall complexity of coal reservoirs. To better reflect the complexities of the pore structures, the fractal dimensions D_5 , D_4 , and D_3 of each aperture segment are calculated for V, IV, and III (see Table 6). The geometric fractal

greater than 3, but the calculation results are still effective evaluation indexes to characterize the heterogeneity of coal pore structure.

4.5. Fractal Dimension Analysis. Due to the error of the mercury injection experiment in the measurement of small pore size, low-temperature liquid nitrogen adsorption cannot measure the large pore size. Therefore, the fractal dimension maps of the two experiments are nested. The pore size of 50 nm is taken as the boundary point, and the fractal dimension integration map is shown in Figure 10.

The fractal dimensions of different types of pores are calculated according to the curve fitting results in Figure 10. The calculation results are shown in Table 7.

The fractal dimension curve is drawn according to the data from Table 7. According to Figure 11, the fractal dimension of tectonic coal is higher than that of primary-structure coal on the whole. Except for classes I and V, the fractal dimensions of tectonic coal are all high, indicating that the pore structure of tectonic coal is more complex than that of primary-structure coal, and the results are similar to those of box fractal dimension. The highest fractal dimension of tectonic coal is type IV pore and that for primary-structure coal is type III pore.

4.6. Coal Sample Pore Size and Specific Surface Area. According to the fractal curve, the pores are divided into five categories: I (< 2 nm), II (2–50 nm), III (50–2000 nm), IV (2000–20 000 nm), and V ($> 20 000$ nm). Among them, I and II are measured by a low-temperature liquid nitrogen adsorption experiment and III, IV, and V are measured by a mercury intrusion experiment. Since gas adsorption mainly occurs in pores, pore volume distributions and specific surface area in the main coal samples are studied. The pore analysis results are shown in Table 8.

Tectonic deformation has a strong transformation effect on the change in the pore structure characteristics of coal. Tectonic deformation increases the porosity of coal. The pore volume of different pore sizes increases with the increase in tectonic deformation, and the change in the pore percentage of different pore sizes is different. The proportion of pores in coal is shown in Table 7. According to Figure 12, the pores of tectonic coal and primary coal are mainly concentrated in type II pores, and the proportion of primary-structure coal is 74.46%, while that of tectonic coal is only 52.70%, which may be due to the following two reasons: (1) tectonic stress causes new pores and cracks in coal, and the increase in type II pores is lower than that of other pores and (2) the proportion is reduced by the collapse or closure of some type II pores due to tectonic stress.

There is a certain correlation between the amount of gas adsorption and the specific surface area of coal samples.

Table 6. Pore Fractal Dimension of Coal^a

sample	pore size range/nm	A	D_i	R^2
TC	$> 20\ 000$	−1.003	2.997	0.94
	20 000–2000	−0.481	3.529	0.95
	2000–50	−0.901	3.099	0.92
PSC	$> 20\ 000$	−1.864	2.136	0.75
	20 000–2000	−0.790	3.210	0.97
	2000–50	−0.745	3.255	0.91

^a D_i is the total identifier of fractal dimension, where the fractal dimension of aperture larger than 20000 nm is D_5 ; 20 000–2000 nm fractal dimension is D_4 ; the fractal dimension of 2000–50 nm aperture is D_3 .

dimensions of the pore V and IV of tectonic coal are higher than that of primary-structure coal, and those of pore III are lower than that of primary-structure coal.

The geometric fractal dimension reflects the complexity of the coal pore surface, and its value should vary between 2 and 3. The larger the fractal dimension, the more complex the pore structure is. A pore fractal dimension equal to 2 represents a relatively uniform pore structure, whereas a fractal dimension equal to 3 represents a highly irregular pore structure. The number of geometric fractal dimensions exceeding 3 may be due to the following reasons: (I) there are voids between coal particles; (II) the pore structure is destroyed; and (III) there are certain cracks in the material. Due to the compression deformation of coal matrix caused by high mercury injection pressure, the calculation results of fractal dimension are often

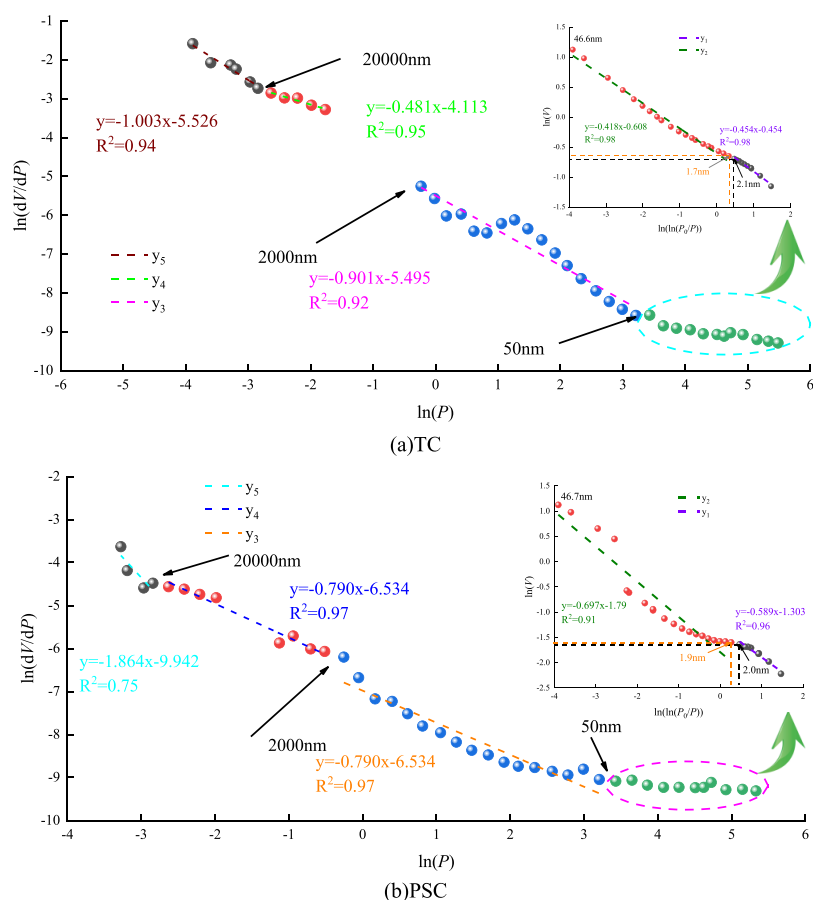


Figure 10. Fractal dimension of different coal samples.

Table 7. Fractal Dimension Summary Table of Different Coal Samples

sample	I 0–2	II 2–50	III 50–2000	IV 2000–20 000	V 20 000~
TC	2.546	2.411	2.997	3.529	3.099
PSC	2.582	2.303	2.136	3.210	3.255

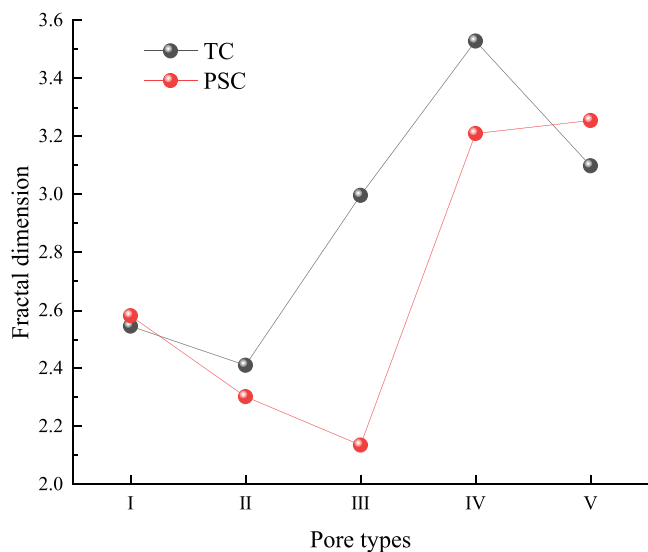


Figure 11. Variation curves of fractal dimension of different coal samples.

Therefore, the curves of pore size and specific surface area of different coal samples are drawn. According to the curves, the specific surface area of tectonic coal is $11.865 \text{ m}^2/\text{g}$ and that of primary-structure coal is $7.382 \text{ m}^2/\text{g}$. The curve is shown in Figure 13.

With the increase in coal crushing degree, the specific surface area of coal increases gradually. This shows that the coal seam geological tectonics aggravate the change in the specific surface area of the coal body. Under geological tectonics, the specific surface area of the coal sample with a higher crushing degree is larger, that is, the coal body has a stronger ability to accommodate gas.

5. CONCLUSIONS

The functional groups, pore diameter, and specific surface area distribution of tectonic coal and primary-structure coal were analyzed through experiments. According to the experimental data of SEM, mercury injection, and nitrogen adsorption, the complexity of internal pores in coal was revealed by fractal theory, and the influence of geological action on coal pores was revealed. The main research results of this paper are as follows:

- (1) The aliphatic functional groups and hydrogen content of tectonic coal are higher than those of aromatic structural functional groups. The content of the straight chain of raw coal is more than that of the side chain. The aliphatic hydrocarbon mostly consists of short chains and has a high branching degree. There are many hydroxyl, carboxyl, and carbonyl groups in primary-structure coal,

Table 8. Coal Sample Pore Volume Distribution

sample	parameter	I	II	III	IV	V	sum
		0–2	2–50	50–2000	2000–20 000	20 000~	NA
TC	V	2.96×10^{-3}	3.47×10^{-2}	1.67×10^{-2}	6.39×10^{-3}	5.09×10^{-3}	0.06575
	V%	4.51	52.70	25.33	9.72	7.73	100
	A	3.55	8.12	1.94×10^{-1}	2.01×10^{-3}	2.89×10^{-4}	11.865
PSC	A%	29.91	68.43	1.63	0.0169	0.00244	100
	V	6.77×10^{-4}	2.01×10^{-2}	4.27×10^{-3}	1.63×10^{-3}	3.25×10^{-4}	0.02703
	V%	2.51	74.46	15.81	6.01	1.20	100
	A	8.05×10^{-1}	6.52	5.27×10^{-2}	7.94×10^{-4}	2.49×10^{-5}	7.382
	A%	10.90	88.38	0.71	0.0108	0.000034	100

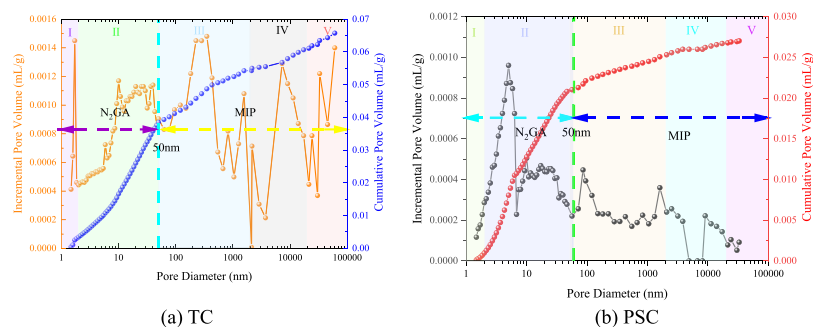


Figure 12. Curves of incremental pore volume and cumulative pore volume varied with the pore diameter of coal samples.

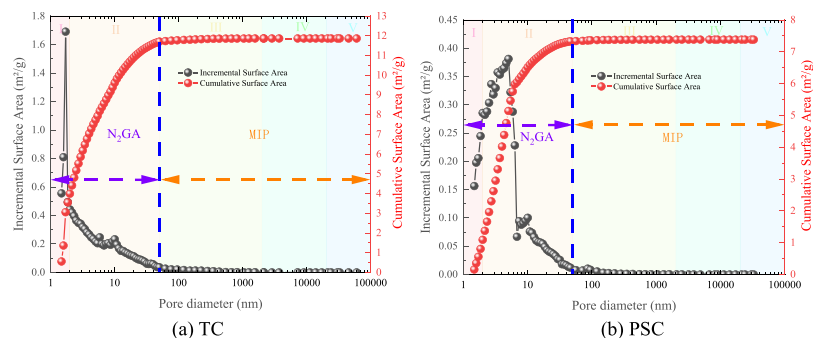


Figure 13. Distribution of the pore-specific surface area.

and the probability of forming hydrogen bonds in coal is high, making it difficult for coal to adsorb gas.

- The pores were divided into five categories (I (<2 nm), II (2–50 nm), III (50–2000 nm), IV (2000–20 000 nm), and V (>20 000 nm)) by mercury intrusion experiment and low-temperature liquid nitrogen experiment. The pore size of primary-structure coal is mainly concentrated in type II pores, and the pore size distribution of tectonic coal is relatively wide, with the majority of them being class I and class II pores. The specific surface area of tectonic coal is 60.7% more than that of primary-structure coal.
- In the box fractal dimension of coal, the box fractal dimension of coal decreases with the increase in SEM magnification. The minimum fractal dimension of tectonic coal is 2.49, which is 7.8% lower than the peak of 2.70. It can be seen from the fractal dimension that the fractal dimensions of pore types II, III, and IV of tectonic coal are higher than those of primary-structure coal.

AUTHOR INFORMATION

Corresponding Author

Shixiang Tian – College of Mining Engineering, Guizhou University, Guiyang 550025 Guizhou, China; The National Joint Engineering Laboratory for the Utilization of Dominant Mineral Resources in Karst Mountain Area, Guizhou University, Guiyang 550025 Guizhou, China; orcid.org/0000-0003-4869-1499; Email: husttsx@163.com

Authors

Huaying Lin – College of Mining Engineering, Guizhou University, Guiyang 550025 Guizhou, China

Anjun Jiao – College of Mining Engineering, Guizhou University, Guiyang 550025 Guizhou, China

Zuoyong Cao – Institute of Mining Engineering, Guizhou Institute of Technology, Guiyang 550000 Guizhou, China; Guizhou Administration of Coal Safety, Guiyang 550000 Guizhou, China

Kai Song – College of Safety and Ocean Engineering, China University of Petroleum, Beijing 102249, China

Yihuai Zou – College of Mining Engineering, Guizhou University, Guiyang 550025 Guizhou, China

Complete contact information is available at:
<https://pubs.acs.org/10.1021/acsomega.2c02222>

Funding

This work was supported by the National Natural Science Foundation of China under Grant number 52104079 and by the Guizhou Provincial Science and Technology Projects under Grant number [2020]4Y050.

Notes

The authors declare no competing financial interest.

ACKNOWLEDGMENTS

The authors appreciate the support from the above funders.

REFERENCES

- (1) Li, X. L.; Cao, Z. Y.; Xu, Y. L. Characteristics and trends of coal mine safety development. *Energy Sources, Part A* **2020**, 1–14.
- (2) Li, X. L.; Chen, S. J.; Li, Z. H.; Wang, E. Y. Rockburst mechanism in coal rock with structural surface and the microseismic (MS) and electromagnetic radiation (EMR) response. *Eng. Failure Anal.* **2021**, *124*, No. 105396.
- (3) Lin, H. Y.; Tian, S. X.; Jiao, A. J.; Zeng, J. H.; Jiang, Z. B.; Xu, S. Q.; Xie, X. G.; Tang, J. Numerical and experimental studies on dynamic gas emission characteristics of boreholes. *PLoS One* **2021**, *16*, No. e0251209.
- (4) Li, X. L.; Chen, S. J.; Zhang, Q. M.; Gao, X.; Feng, F. Research on theory, simulation and measurement of stress behavior under regenerated roof condition. *Geomech. Geoeng.* **2021**, *26*, 49–61.
- (5) Li, X. L.; Chen, S. J.; Liu, S. M.; Li, Z. H. AE waveform characteristics of rock mass under uniaxial loading based on Hilbert-Huang transform. *J. Cent. South Univ.* **2021**, *28*, 1843–1856.
- (6) Liu, S. Q.; Sang, S. X.; Wang, G.; Ma, J. S.; Wang, X.; Wang, W. F.; Du, Y.; Wang, T. FIB-SEM and X-ray CT characterization of interconnected pores in high-rank coal formed from regional metamorphism. *J. Pet. Sci. Eng.* **2017**, *148*, 21–31.
- (7) Song, Y.; Xie, J.; Fu, H.; Xin, L. Pore fractal characteristics of lignite at different temperatures based on mercury intrusion test. *Geotech. Geol. Eng.* **2019**, *37*, 4837–44.
- (8) Rouquerol, J.; Gino, V. B.; Renaud, D.; Herbert, G.; Johan, G.; Peter, K.; Pierre, L.; Alexander, V. N.; Sean, R.; Romas, S.; et al. The characterization of macroporous solids: an overview of the methodology. *Microporous Mesoporous Mater.* **2012**, *154*, 2–6.
- (9) Pan, J. N.; Wang, S.; Ju, Y. W.; Hou, Q. L.; Niu, Q. H.; Wang, K.; Li, M.; Shi, X. H. Quantitative study of the macromolecular structures of tectonically deformed coal using high-resolution transmission electron microscopy. *J. Nat. Gas Sci. Eng.* **2015**, *27*, 1852–62.
- (10) Li, H. Y.; Yue, D. L.; Zhang, X. J. Characteristics of pore structure and reservoir evaluation of low permeability reservoir in Sulige gas field. *Earth Sci. Front.* **2012**, *19*, No. 133e40.
- (11) Cheng, Z. H.; Li, W. H.; Xue, H. T.; Lu, S. F.; Tan, Z. H. Grading evaluation criteria of tight sandstone reservoir based on high pressure mercury injection technology and fractal theory. *J. Northeast Pet. Univ.* **2019**, *43*, No. 50e9.
- (12) Hofmann, C. C.; Gregor, H. J. Scanning electron microscope and light microscope investigations of pollen from an atypical mid-Eocene coal facies in Stolzenbach mine (PreußenElektra) near Borken (Kassel, Lower Hesse, Germany). *Rev. Palaeobot. Palynol.* **2018**, *252*, 41–63.
- (13) Creelman, R. A.; Colin, R. W. A scanning electron microscope method for automated, quantitative analysis of mineral matter in coal. *Int. J. Coal Geol.* **1996**, *30*, 249–269.
- (14) Blunt, M. J.; Branko, B.; Hu, D.; Oussama, G.; Stefan, I.; Peyman, M.; Adriana, P.; Christopher, P. Pore-scale imaging and modelling. *Adv Water Resour.* **2013**, *51*, 197–216.
- (15) Lemmens, H. J.; Butcher, A. R.; Botha, P. W. S. K. In *FIB/SEM and Automated Mineralogy for Core and Cuttings Analysis*, SPE Russian Oil and Gas Conference and Exhibition, SPE: Moscow, Russia, 2010; 136327.
- (16) Pan, J.; Hou, Q.; Ju, Y.; Bai, H.; Zhao, Y. Coalbed methane sorption related to coal deformation structures at different temperatures and pressures. *Fuel* **2012**, *102*, 760–765.
- (17) Li, W.; Liu, H.; Song, X. Multifractal analysis of hg pore size distributions of tectonically deformed coals. *Int. J. Coal Geol.* **2015**, *144–145*, 138–152.
- (18) Wang, Z. Y.; Cheng, Y. P.; Qi, Y. X.; Wang, R. P.; Wang, L.; Jiang, J. Y. Experimental study of pore structure and fractal characteristics of pulverized intact coal and tectonic coal by low temperature nitrogen adsorption. *Powder Technol.* **2019**, *350*, 15–25.
- (19) Liu, Y. W.; Zhang, X. M.; Miao, J. Study on Evolution of Pore Structure of Medium and High Rank Coals. *Saf. Coal Mines.* **2020**, *51*, 7–13.
- (20) Chen, X. J.; Zhao, S.; Si, Z. X.; Qi, L. L.; Kang, N. N. Fractal characteristics of pore structure of coal with different metamorphic degrees and its effect on gas adsorption characteristics. *Coal Sci. Technol.* **2020**, *48*, 118–124.
- (21) Mangi, H. N.; Yan, D.; Nayima, H.; Umar, A.; Riaz, H. R. Pore structure characteristics and fractal dimension analysis of low rank coal in the Lower Indus Basin, SE Pakistan. *J. Nat. Gas Sci. Eng.* **2020**, *77*, No. 103231.
- (22) Tu, Q. *Study on Apparent Physical Structure of Tectonic Coal and Spallation Development Mechanism of Coal and Gas Outburst*; China University of Mining and Technology, 2019.
- (23) Ye, Z. N.; En, K. H.; Duan, Z. H.; Wen, Q.; Huang, M. T. Fractal characteristics of pores and microfractures of coals with different structure and their effect on permeability. *Coal Geol. Explor.* **2019**, *47*, 70–78.
- (24) Mahamud, M. M.; Novo, M. F. The use of fractal analysis in the textural characterization of coals. *Fuel* **2008**, *87*, 222–231.
- (25) Xu, S. Q.; Zhou, Z. J.; Yu, G. S.; Wang, F. C. Effects of pyrolysis on the pore structure of four Chinese coals. *Energy. Fuel* **2010**, *24*, 1114–1123.
- (26) Mahamud, M.; López, Ó.; Pis, J. J.; Pajares, J. A. Textural characterization of coals using fractal analysis. *Fuel Process. Technol.* **2003**, *81*, 127–142.
- (27) Chengyang, W.; Hao, S. X.; Sun, W. J.; Chu, W. Fractal dimension of coal particles and their CH₄ adsorption. *Int. J. Min. Sci. Technol.* **2012**, *22*, 855–858.
- (28) Song, H.; Li, M.; Xiang, J.; Sun, L. S.; Li, P. S.; Su, S.; Sun, X. X. Fractal characteristic of three Chinese coals. *Fuel* **2004**, *83*, 1307–1313.
- (29) Xu, P.; Mujumdar, A. S.; Yu, B. M. Fractal theory on drying: a review. *Dry. Technol.* **2008**, *26*, 640–650.
- (30) Yang, F.; Ning, Z. F.; Liu, H. Q. Fractal characteristics of shales from a shale gas reservoir in the Sichuan Basin, China. *Fuel* **2014**, *115*, 378–384.
- (31) Jiao, A.; Tian, S. X.; Lin, H. Y. Analysis of Outburst Coal Structure Characteristics in Sanjia Coal Mine Based on FTIR and XRD. *Energies* **2022**, *15*, 1956.
- (32) Wang, C. J.; Yang, S. Q.; Li, X. W.; Li, J. H.; Jiang, C. L. Comparison of the initial gas desorption and gas-release energy characteristics from tectonically-deformed and primary-undeformed coal. *Fuel* **2019**, *238*, 66–74.
- (33) Mandelbrot, B. B.; Blumen, A. Fractal Geometry: What is it, and What Does it do? *Proc. R. Soc. London, Ser. A* **1989**, *423*(1864), 3–16.
- (34) Han, W. B.; Zhou, G.; Gao, D. H.; Zhang, Z. X.; Wei, Z. Y.; Wang, H. T.; Yang, H. Q. Experimental analysis of the pore structure and fractal characteristics of different metamorphic coal based on mercury intrusion-nitrogen adsorption porosimetry. *Powder Technol.* **2020**, *362*, 386–398.